

Point defect sink strength of low-angle tilt grain boundaries: a phase field dislocation climb model

Pengchuang Liu^{a,1}, Songlin Zheng^{b,1}, Kaiguo Chen^b, Xin Wang^a, Biaojie Yan^a,
Pengcheng Zhang^{a,*}, San-Qiang Shi^{c,d**}

- a. *Institute of Materials, China Academy of Engineering Physics, 621908 Jiangyou, Sichuan, China*
- b. *National Key Laboratory of Shockwave Physics and Detonation Physics, Institute of Fluid Physics, China Academy of Engineering Physics, 621900 Mianyang, Sichuan, China*
- c. *The Hong Kong Polytechnic University Shenzhen Research Institute, Shenzhen, China*
- d. *Department of Mechanical Engineering, The Hong Kong Polytechnic University, Hung Hom, Kowloon, Hong Kong, China;*

Abstract: Evaluating the point defect sink strength of grain boundaries is crucial for understanding the metal behavior of plasticity and damage under irradiation. In this paper, the point defect sink strength of low-angle symmetrical tilt grain boundaries is investigated by the phase field dislocation climb model under irradiation. The results indicate that sink strength of grain boundary is not only determined by the long-range point defect diffusion but also the short-range point defect absorption by the dynamic climbing of grain boundary dislocations. All of the study findings prove that the irradiation induced creep deformation of grain boundaries is essential for evaluating the radiation tolerance of materials.

Key words: point defects, grain boundaries, dislocation climb, sink strengths

1. Introduction

The accumulation of point defects (PDs) in metals under an irradiated environment

* Corresponding author.

** Corresponding author.

E-mail addresses: 13981102769@163.com (P.C. Zhang); mmsqshi@polyu.edu.hk (S.Q. Shi).

¹ Pengchuang Liu and Songlin Zheng contributed equally to this work.

could cause undesirable changes such as swelling, embrittlement, and creep (Misra et al., 2007; Odette et al., 2008; Bai et al., 2010, Bringa et al., 2011, Kenik and Busby, 2012). Nanocrystalline materials are considered radiation tolerant materials, because the plentiful grain boundaries (GBs) in materials can act as potent sinks for PDs (Was, 2007; Bai et al., 2010; Demkowicz et al., 2012; Wan et al., 2014; Beyerlein et al., 2015; Yu and Shen, 2016). Hence, evaluating the capability of a GB for absorbing PDs is primarily important for the design of radiation resistant materials and understanding the deformation behaviors of such materials.

The ability of a GB to absorb PDs can be characterized by the GB sink strength, and the factors that affect GB sink strength rely on the mechanisms of GBs interacting with PDs and PDs diffusion. Atomistic simulations are powerful tools for investigating the PD-GB interaction and for acquiring some basic thermodynamic and kinetic parameters (Bai et al., 2012; Millett et al., 2009; Tschopp et al., 2012; Zhang et al., 2012). However, the fundamental understandings obtained from these atomistic modeling are difficult to use directly for radiation-resistant material design (Han et al., 2012), due to the limited length scale. Thus, it is necessary to develop a continuum model combined with the atomistic information to predict the GB sink strength effectively (Beyerlein et al., 2015; Zhang et al., 2012).

Most of the existing studies about the continuum models of GB sink strength are theoretical investigations. Grain boundaries are regarded as perfect planar sinks in these studies (where the PD concentration is set to be the thermal equilibrium value) (Was, 2007). However, many experiments have proven that sink properties of different kinds of GBs are significantly different. The experimental observations of the void-denuded zones formed near GBs reveal that the influencing factors of GB sink efficiencies are the overall GB characteristics and that both those of the GB plane orientation and misorientation should be considered (Han et al., 2012). Therefore, the GB-character dependence must be studied in the continuum model to investigate GB sink strength.

The structures of low-angle GBs are well understood and can be fully described by

lattice dislocations. The sink behavior of GB-character dependence could be investigated based on the dislocation models of low-angle GBs. The simplest boundary is the low-angle symmetric tilt GB, where the GB structure is only one set of edge dislocations, and the PDs are absorbed by the GB via climb of such edge dislocations. By using the dislocation models of GBs, the analytical expression of a low-angle symmetric tilt GB sink efficiency can be derived without considering the elastic interaction between PDs and dislocations (Gu et al., 2017). On the other hand, numerical simulations combined with elastic theory of dislocations have been employed to explore the effect of GB stresses on the sink strength, resulting in a surprising conclusion that the sink strengths of high-angle GBs could be lower than low-angle GBs (Jiang et al., 2014). The dislocation-based models offer useful insights into the relationship between the GB sink strength and GB structure. However, most of these models assumed that dislocations at GBs are ideal sinks for PDs in which the PD concentration is fixed at a value derived from the climb mechanism (Gu et al., 2017) or corresponding to the thermal equilibrium state (Jiang et al., 2014; Rouchette et al., 2014) within the dislocation cores, and the dislocations are immobile. This assumption ignores the short-range interaction and dynamic motion of the dislocations during PDs absorption, and therefore the sink strength is determined only by the PD long-range diffusion.

The climb of GB dislocations has a significant impact on the mechanical behavior of nanomaterials (Bobylev et al., 2010; Wang et al., 2014). Temperature-dependent deformations of crystals studied by crystal plasticity models, including the climb mechanism, also emphasize the importance of the diffusion-assisted dislocation motion (Lebensohn et al., 2010; Fischer and Svoboda, 2011; Basirat et al., 2012; Babu and Lindgren, 2013; Geers et al., 2014). As an effective tool to simulate plasticity at the scale of individual dislocations, discrete dislocation dynamics have been used to combine dislocation-climb and vacancy-diffusion (Mordehai et al., 2008; Gao et al., 2011; Davoudi et al., 2012; Keralavarma et al., 2012; Ayas et al., 2014; Huang et al.,

2014; Niu et al., 2017). However, the vacancy diffusion is controlled by the linear equation and the steady-state climb conditions in most of these methods. At the relevant scale, the phase field model (PFM) can be used as another simulation technique to study the dislocation dynamics (Levitas et al., 2010; Wang and Li, 2010; Beyerlein and Hunter, 2016; Zeng et al., 2016; Zheng et al., 2015, 2018). Additionally, microstructure evolutions under irradiated conditions have been effectively predicted by PFM (Li et al., 2017). Recently, the PFM of dislocation climb that couples non-conservative dislocation motion with PD diffusion was developed to allow the removal of the ideal sink assumption for dislocations (Geslin et al., 2014; Ke et al., 2014). In addition, Shen et al. (2014) advanced the PFM of dislocation to describe a low-angle twist GB. In this study, we extended Shen's dislocation model to describe the low-angle symmetrical tilt GBs and then applied it to evaluate the GB sink strength under the irradiation conditions through the PFM of dislocation climb. We will show that GB sink strength is not only determined by the PD diffusion but also the reaction rate of PDs absorption by the dislocations climb, and the transition from reaction-controlled to diffusion-controlled sink processes is also presented. By comparing with the results obtained from the ideal sink model, it is found that the dynamics of the dislocation motion during PD absorption has significant effects on the GB sink strength.

The structure of this article is as follows. The PFM of dislocation is extended to describe the low-angle tilt GBs in section 2. In section 3, we apply this phase field description of GBs to compute the GB sink strength using the PFM of dislocation climb and compare the results to that obtained from the ideal sink model of dislocations. Finally, the main conclusions are summarized.

2. PFM of dislocation for low-angle tilt GBs

2.1 PFM of dislocation

In the PFM of dislocation, the amount of relative slips at position \mathbf{r} is represented

by the non-conserved phase field variables $\eta(\alpha, m_\alpha, \mathbf{r})$ in units of Burgers vector $\mathbf{b}(\alpha, m_\alpha)$, where α represents the slip plane and m_α is the glide direction. The slipped and unslipped parts correspond to regions with $\eta(\alpha, m_\alpha, \mathbf{r}) \neq 0$ and $\eta(\alpha, m_\alpha, \mathbf{r}) = 0$ in a crystal, respectively. Boundaries of the slipped and unslipped regions are regarded as dislocation lines. Dislocation assembly can be expressed through the evolution of $\eta(\alpha, m_\alpha, \mathbf{r})$, and the process is controlled by decreasing the total free energy toward the minimum. Total free energy is composed of elastic energy, crystalline energy and gradient energy. Following the work regarding the PFM for twist grain boundaries (Shen et al., 2014), we also neglected the gradient energy and restrict the Burgers vector distribution within the glide planes by assuming that $\eta(\alpha, m_\alpha, \mathbf{r}) \equiv 0$ at the point $\mathbf{r} \neq \mathbf{r}_\alpha$, where \mathbf{r}_α is the position vector on the slip plane α . Hence the total energy equals elastic energy plus crystalline energy:

$$E^{tot} = E^{ela} + E^{cry}. \quad (1)$$

Khachaturyan-Shatalov (KS) microelasticity theory was used to calculate the elastic energy based on the eigenstrain $\varepsilon_{ij}^0(\mathbf{r})$ and the external stress. The eigenstrain induced by inelastic slip can be expressed as

$$\varepsilon_{ij}^0(\mathbf{r}) = \sum_{\alpha, m_\alpha} \frac{b_i(\alpha, m_\alpha) n_j(\alpha) + b_j(\alpha, m_\alpha) n_i(\alpha)}{2d_\alpha} \eta(\alpha, m_\alpha, \mathbf{r}), \quad (2)$$

where $n_j(\alpha)$ is the component of the unit normal vector of the slip plane α , and d_α is interplanar distance of these slip planes. Elastic energy yields

$$E^{ela} = \frac{1}{2} \int_{|\xi| \neq 0} \left[C_{ijkl} \tilde{\varepsilon}_{ij}^0(\xi) \tilde{\varepsilon}_{kl}^0(\xi)^* - e_i \tilde{\sigma}_{ij}^0(\xi) \Omega_{jk}(\mathbf{e}) \tilde{\sigma}_{kl}^0(\xi)^* e_l \right] \frac{d^3 \xi}{(2\pi)^3} - \int \sigma_{ij}^{ext} \varepsilon_{ij}^0(\mathbf{r}) d^3 r - \frac{V}{2} C_{ijkl}^{-1} \sigma_{ij}^{ext} \sigma_{kl}^{ext}, \quad (3)$$

where C_{ijkl} is the elastic moduli tensor, ξ represents the Fourier space vector, and $\mathbf{e} = \xi / |\xi|$ indicates unit vector along ξ . $\tilde{\varepsilon}_{ij}^0(\xi) = \int \varepsilon_{ij}^0(\mathbf{r}) e^{-\xi \cdot \mathbf{r}} d^3r$ is the Fourier transformation of $\varepsilon_{ij}^0(\mathbf{r})$, and $\tilde{\sigma}_{ij}^0(\xi) = C_{ijkl} \tilde{\varepsilon}_{kl}^0(\xi)$. $\Omega_{jk}(\mathbf{e}) = (C_{jlpk} e_l e_p)^{-1}$ is the elastic Green function, and the symbol $*$ represents complex conjugation. $\int_{|\xi| \neq 0}$ is an integral in Fourier space excluding the point of $|\xi| = 0$, V is the system volume, and σ_{ij}^{ext} is the external applied stress. After substituting Eq. (2) into Eq. (3), the elastic energy can be expressed by the field parameters in Fourier space.

The periodical potential f^{cry} was used to describe the misfit energy of the local disregistry within the core. Thus, the crystalline energy is given as follows:

$$E^{cry} = \int f^{cry} d^3r. \quad (4)$$

The expression of f^{cry} is always expanded to be a Fourier-series, but a simplified approximation is used here by following the periodic Peierls potential:

$$f^{cry} = \sum_{\alpha, m_\alpha} \frac{A}{d_\alpha} \sin^2 \pi \eta(\alpha, m_\alpha, \mathbf{r}), \quad (5)$$

where A represents the approximate stacking fault energy for the corresponding slip system.

As both types of energies are expressed by the phase field variables, the dislocation dynamics is determined by the time-dependent Ginzburg-Landau (TDGL) equation:

$$\frac{\partial \eta(\alpha, m_\alpha, \mathbf{r}, t)}{\partial t} = -L \frac{\delta E^{tot}}{\delta \eta(\alpha, m_\alpha, \mathbf{r}, t)}, \quad (6)$$

where L is the positive kinetic coefficient related to the dislocation mobility characterizing the relaxation rate of the phase fields. Based on the thermal activation theory of dislocations, we can estimate $L = L_0 \exp(-\Delta E / k_B T)$, where ΔE is

activation energy, k_B is the Boltzmann constant, T is the kelvin temperature, and L_0 is a coefficient independent of temperature. The equilibrium state of a dislocation is achieved when $\delta E^{tot} / \delta \eta(\alpha, m_\alpha, \mathbf{r}) = 0$.

2.2 Low-angle symmetrical tilt GBs

Shen et al. (2014) developed the PFM of dislocation to describe pure twist GBs. A similar method was adopted here to deal with the low-angle symmetrical tilt GBs. A symmetrical tilt grain boundary can be constructed by a perfect crystal with the following steps shown in Fig. 1: (1) the perfect crystal is cut into two half crystals along the y axis in the coordinate (Fig. 1a); (2) a rigid-body rotation of the left half crystal relative to the right one is introduced, the rotation angle is θ , and the rotation axis is the z axis (Fig. 1b); (3) the crystal is completed by removing the overlap and filling up the vacant part so that the crystal lattice is perfect except in the region of $x = 0$ (Fig. 1c), and the displacement of the region of $x = 0$ is induced by the rigid-body rotation and expressed as $\mathbf{u}^R(x=0)$; and (4) the non-perfect region of $x = 0$ is locally relaxed to the minimum energy state and the relaxation displacement is \mathbf{v} . After the four steps, a bi-crystal with an equilibrium symmetrical tilt GB located in the region $x = 0$ is generated. The total displacement of the boundary $\mathbf{u}^{tot} = \mathbf{u}^R + \mathbf{v}$ should be calculated for describing the boundary's structure.

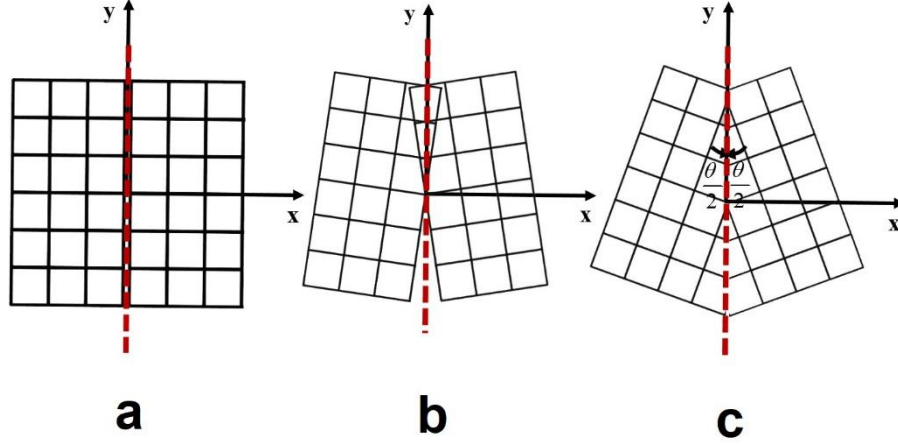


Fig. 1 Schematic diagram of the steps for constructing a symmetrical tilt grain boundary.

The displacement of the rigid-body rotation in two-dimensional space is (Shen et al., 2014):

$$\mathbf{u}^R(\mathbf{r}) = [\mathbf{R}(\theta/2) - \mathbf{R}(-\theta/2)]\mathbf{r}, \quad (7)$$

where R is the rotation matrix expressed as: $\mathbf{R}(\omega) = \begin{pmatrix} \cos \omega & \sin \omega \\ -\sin \omega & \cos \omega \end{pmatrix}$. It is given

that $\mathbf{u}^R = (y\theta, -x\theta, 0)$ in three-dimensional space when GB is low-angle with $\theta \ll 1$.

For the region $x=0$, $\mathbf{u}^R(x=0) = (y\theta, 0, 0)$. Because the relaxation displacement is caused by the rigid-body rotation, the total displacement only contains the component along the x axis. Then the boundary can be considered an array of parallel pure-edge dislocations, and the Burgers vector is $\mathbf{b} = (-b, 0, 0)$. The edge dislocations are strictly confined within the slip plane $x=0$, and the unit normal vector is $\mathbf{n} = (1, 0, 0)$. We use the field variables to represent the amount of relative displacements to the Burgers vector: $\mathbf{u}^{tot} = \eta^{tot}(\mathbf{r})\mathbf{b}$, $\mathbf{u}^R = \eta^R(\mathbf{r})\mathbf{b}$ and $\mathbf{v} = \eta(\mathbf{r})\mathbf{b}$. The field variables are non-zero only within the boundary with $\eta^R = \theta y \delta(x) / b$ and $\eta^{tot} = \eta^R + \eta$, where $\delta(x)$ is the Dirac function on the GB plane.

It is reasonable to describe the tilt boundary energy by the dislocation model.

Crystalline energy is the misfit energy induced by the total displacement:

$$E^{cry} = E^{cry}(\eta^{tot}) = E^{cry}(\eta^R + \eta). \quad (8)$$

In this situation, the Burgers vector is vertical to the slip plane, and the edge dislocations are prismatic-type. Therefore, the crystalline energy density function f^{cry} should be different from the one for the glide-type dislocations. However, the crystals remain complete because of the assistance of the PD absorption during the dislocation motion; the completeness ensures that f^{cry} is still a periodical function. Thus, we used the simplified approximation expression from Eq. (5) to describe the misfit energy of the (100) boundary of the cubic crystal:

$$E^{cry} = \int \frac{A}{d} \sin^2 \pi(\eta^R + \eta) d^3 r. \quad (9)$$

The elastic energy is given by Eq. (3) as a function of the eigenstrain. Since rigid-body rotation does not cause elastic strain, the eigenstrain is determined only by the field variable associated with the relaxation displacement:

$$\varepsilon_{ij}^0 = \frac{b_i n_j + b_j n_i}{2d} \eta. \quad (10)$$

Combining Eqs. (9) and (10) with Eqs. (1) and (3), the total energy is dependent on two field variables: η^R and η . For a fixed rotation angle θ , $\eta^R \equiv y\theta\delta(x)/b$ and only η needs to be determined by the TDGL equation (Eq. (6)) during the relaxation:

$$\frac{\partial \eta}{\partial t} = -L \frac{\delta E^{tot}}{\delta \eta} = -L \frac{\delta [E^{cry}(\eta^R + \eta) + E^{ela}(\eta)]}{\delta \eta}, \quad (11)$$

The initial state is $\eta = 0$ (or $\eta^{tot} = \eta^R = y\theta\delta(x)/b$), and the equilibrium state is achieved when $\delta E^{tot} / \delta \eta$ reaches zero. The crystal is assumed to be elastic

isotropic, and we use the material parameters of metal aluminum (see Table 1). Eq. (11) can be solved numerically in reduced form with all physical lengths measured in units of b , all the stresses in units of μ (the shear modulus) and the time in units of t_0 . The simulations are performed using the periodic boundary conditions without external applied stress.

The simulated structure of the $\theta = 2.86^\circ$ tilt boundary in the computational cell of $80b \times 80b \times 2b$ is shown in Fig. 2. The profiles of η^{tot} with respect to y/b along the boundary $x=0$ at the initial state and equilibrium state are plotted in Fig. 2a. At the initial state, the profile is a straight line corresponding to $\eta^{tot} = \eta^R = y\theta/b$. After relaxation, η^{tot} is composed of segmented constants and sudden jumps at the equilibrium state, which is similar to the results calculated by Dai et al. for the twist boundaries (Dai et al., 2013). The regions of constant η^{tot} are perfect lattices, and the jumps between them are dislocations. As shown in Fig. 2a, the distances between the neighboring jumps are the same, and the calculated value is $h = 20b$, which is nearly equal to the theoretical value of $b/\theta = 20b$. Fig. 2b plots the crystal energy density f^{cry} at the equilibrium; the figure clearly shows that the grain boundary consists of a series of parallel edge dislocations with a fixed separation distance of $h = 20b$ according to the periodical boundary condition. The simulated results show good agreement with the theoretical studies, indicating that the model adopted here is valid for describing the structures of low-angle symmetrical tilt GBs.

It is worth noting that only the (100) symmetrical tilt GB is constructed here in the phase field dislocation model. This model can be extended easily to describe arbitrary planar low-angle pure twist or pure tilt GBs. When the cut plane (GB plane) is perpendicular to the rotation axis, the GB type is pure twist, and the general model has been carefully discussed by Shen et al. (2014). If the cut plane is parallel to the rotation axis, this plane will be a pure tilt GB. In particular, while the rotation axis is located in

the cut plane, the GB is a symmetric tilt plane. Thus, the rigid rotation processes are all the same for the symmetric tilt GBs with different crystallographic orientations. However, the relaxation process is dependent on the crystallographic orientation of the GB plane. In this study, a (100) symmetric tilt GB in a cubic crystal is considered, and the simple sinusoidal function of Eq. (9) is employed to describe the crystalline energy. For the GBs with other crystallographic orientations, the *ab initio* generalized stacking fault energy (GSFE) function similar to the γ surface of such a crystallographic slip plane must be used to replace Eq. (9) for calculating the crystalline energy. Different GSFE functions will lead to different dislocation patterns. For instance, dislocation dissociations and partial dislocations may appear in a (111) symmetric tilt GB in a face-centered cubic crystal.

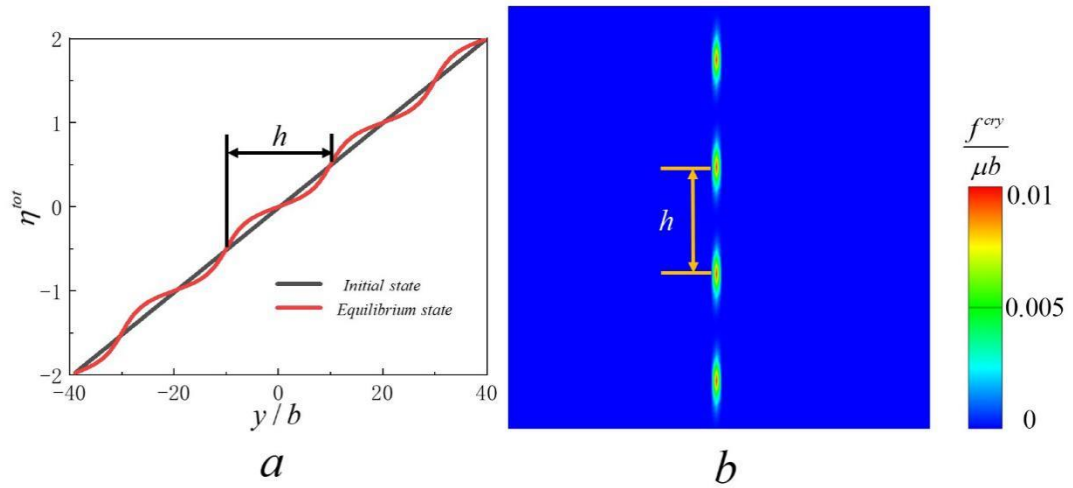


Fig. 2 Simulated structure of the $\theta = 2.86^\circ$ tilt grain boundary in the computational cell of $80b \times 80b \times 2b$. **a.** Plots of η^{tot} with respect to y/b along the boundary $x=0$ at the initial state and equilibrium state. **b.** Plots the crystal energy density f^{cry} at the equilibrium state.

3. Sink strengths of low-angle tilt GBs

In this section, the PFM of the dislocation climb was employed to calculate the sink

strengths of the low-angle tilt GBs generated in section 2, and the results are compared to that of the ideal sink model of dislocations. The PFM of dislocation climb and the ideal sink model are introduced in section 3.1, and the results are shown in section 3.2.

3.1 Model descriptions

3.1.1 PFM of dislocation climb

Geslin et al. (2014) and Ke et al. (2014) have developed the PFM to describe discrete climbing dislocations. Here, we applied this model to research the sink of PDs via the climb of the parallel edge dislocations in GBs. For simplicity, we assumed that only one type of PD, vacancy, exists to exclude the mutual recombination among different point defects. The conserved phase field variable $c(r)$ was adopted to denote the vacancy concentration, and the parameters η^R and η calculated in the former section are used to represent the GB dislocations. The total energy, F^{tot} , includes three terms: the chemical energy of vacancy F^{chem} , the elastic strain energy F^{ela} and the crystalline energy of dislocations F^{cry} . The chemical free energy employs the ideal solution model:

$$F^{chem} = \frac{1}{V_m} \int \{ E^f c(1-c) + k_B T [c \ln c + (1-c) \ln(1-c)] \} d^3 r, \quad (12)$$

where V_m is the atomic volume and E^f is the vacancy formation energy. The elastic energy F^{ela} is calculated using Eq. (3), and the eigenstrain here includes contributions from dislocations and vacancies:

$$\varepsilon_{ij}^0 = \frac{b_i n_j + b_j n_i}{2d} \eta + \frac{\Delta V}{3V_m} c \delta_{ij}, \quad (13)$$

where ΔV is the vacancy relaxation volume and δ_{ij} is the Kronecker delta. The crystalline energy of the dislocation F^{cry} is given in Eq. (9). Thus, the total energy

consisting of these three energy terms is directly determined by three phase field variables.

For a given tilt angle, the variable η^R is invariable with respect to time ($\eta^R \equiv \theta y \delta(x)/b$); therefore, only the parameters η and c need to be evaluated during the sink process. Eq. (11) gives the controlling equation for the non-conserved variable η . However, an additional contribution should be considered: the osmotic force caused by the vacancy concentration deviating from the equilibrium value. Researchers have derived the osmotic force as $f^{osm} = -\mu_v b / V_m$, where $\mu_v = V_m \delta F^{chem} / \delta c$ is the vacancies chemical potential. Thus, the TDGL equation for the dislocation climb is (Ke et al., 2014)

$$\frac{\partial \eta}{\partial t} = -L \left[\frac{\delta F^{tot}}{\delta \eta} + \frac{f^{osm}}{b} \right] = -L \left[\frac{\delta F^{tot}}{\delta \eta} - \frac{\delta F^{chem}}{\delta c} \right]. \quad (14)$$

The long-range diffusion of vacancies is controlled by the Cahn-Hilliard equation, and the short-range vacancy absorption arises from the dislocation climb. Under irradiation, the evolution equation containing reaction-diffusion mechanism is given by:

$$\frac{\partial c}{\partial t} = \nabla \cdot M \nabla \frac{\delta F^{tot}}{\delta c} - \frac{\partial \eta}{\partial t} + K_0, \quad (15)$$

where M is the vacancy mobility coefficient, which can be expressed as $M = V_m D c (1-c) / (k_B T)$, $D = D_0 \exp(-E^m / k_B T)$ is the vacancy diffusion coefficient, D_0 is the pre-exponential factor, E^m is the vacancy migration energy, and K_0 is the vacancy generation rate. The first term in this equation describes the vacancy diffusion, which is consistent with the Cahn-Hilliard equation. The second term represents the vacancy absorption, and the absorbing process is accompanied by a dislocation climb. The third term is the vacancy generation term due to the radiation. It

should be noted that no other internal sinks are assumed to exist in the grain in order to isolate the effects of the GB.

Additionally, it is necessary to point out that uniform E^f and E^m are adopted here in this 2D dislocation climb model for simplicity. However, E_c^f (vacancy formation energy in the dislocation core) is verified to be lower than E_b^f (such energy in the bulk), indicating that the thermal equilibrium vacancy concentration within the dislocation core is higher than that in the bulk. On the other hand, pipe diffusion of vacancies along the dislocation line is much faster than bulk diffusion, revealing that E_c^m (vacancy migration energy in the dislocation core) is much smaller than E_b^m (such energy in the bulk). These phenomena would have significant effects on the diffusion processes and dislocation climb dynamics when this model is extended into the 3D framework. For this case, we could employ $E^f = E_b^f + (E_c^f - E_b^f) f^{cry} / A$ and $E^m = E_b^m + (E_c^m - E_b^m) f^{cry} / A$ to reflect the non-uniform vacancy formation energy and anisotropic diffusion energy barriers, respectively.

3.1.2 Ideal sink model

In the ideal sink model, the dislocations are immobile and the PD concentration of the dislocation core region is fixed at a constant value. Following the work of Rouchette et al. (2014), another order parameter $\lambda(r)$ is incorporated into this model to express the capture zones of the sinks, which is set to be 1 within the dislocation cores and 0 outside, as shown in Fig. 3. In contrast to the circular dislocation cores adopted by Misra et al. (2007), Jiang et al. (2014) and Rouchette et al. (2014), the shape of the dislocation cores here are assumed to be line segments, corresponding to the dislocation structures shown in Fig. 2b. The length of the line segments should be equal to the dislocation core width $2w$, and it can be determined by:

$$\frac{w}{w_0} = \frac{A_0}{A}, \quad (16)$$

with the core width $2w_0 = d / (1 - \nu)$ and $A_0 = \mu b^2 / (2\pi^2 d)$ in the original Peierls-Nabarro model. Since $A = 0.01\mu b$ is chosen here, then $w = 3.62b$.

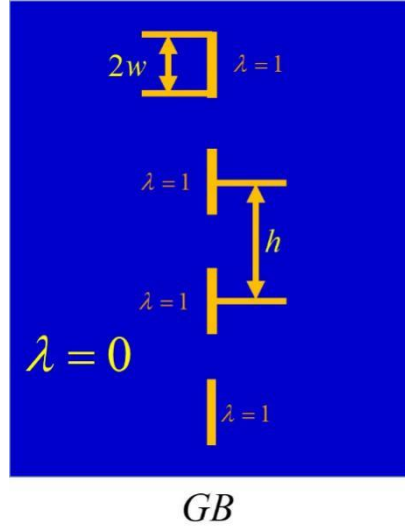


Fig. 3 Schematic diagram of the ideal sink model. The orange line segments with $\lambda = 1$ represent the regions within the dislocation cores.

Since climb of the dislocations is ignored here, the parameters λ and η are invariable with respect to time. The sink process is determined only by the vacancy diffusion:

$$\frac{\partial c}{\partial t} = \nabla \cdot M \nabla \frac{\delta F^{tot}}{\delta c} - \frac{\lambda}{\Delta t} (c - c^{th}) + K_0, \quad (17)$$

where Δt is the calculation time step and $c^{th} = \exp(-E^f / k_B T)$ is the thermal equilibrium vacancy concentration. Replacing the vacancy absorption term induced by the dislocation climb in Eq. (15), the second term of Eq. (17) in the right side was proposed by Jiang et al. (2014) and Rouchette et al. (2014). This absorption term was set to zero in the system except in the zones of the dislocation cores, ensuring that the vacancy concentration was fixed at c^{th} within the capture zone of the sinks.

3.1.3 Parameters

Table 1 Simulation parameters.

Parameters	Value	References
Burgers vector, \mathbf{b}	0.285 nm	Geslin et al. (2014)
Interplanar distance, \mathbf{d}	0.285 nm	Geslin et al. (2014)
Shear modulus, μ	26 GPa	Geslin et al. (2014)
Poisson ratio, ν	0.3	This work
Stacking fault energy, \mathbf{A}	74.1 mJ/m ²	Beyerlein and Hunter (2016)
Time, \mathbf{t}_0	3.23×10^{-11} s	Geslin et al. (2014)
Kinetic coefficient, \mathbf{L}	0.0064 m ³ /J s	Geslin et al. (2014)
Atomic volume, \mathbf{V}_m	0.0164 nm ³	Geslin et al. (2014)
Vacancy formation energy, \mathbf{E}^f	0.67 eV	Geslin et al. (2014)
Vacancy migration energy, \mathbf{E}^m	0.61 eV	Geslin et al. (2014)
Temperature, \mathbf{T}	812 K	Geslin et al. (2014)
Vacancy relaxation volume, $\Delta\mathbf{V}$	$-0.15 \times V_m$	Ke et al. (2014)
Pre-exponential factor, \mathbf{D}_0	1.51×10^{-5} m ² /s	Geslin et al. (2014)
Dose rate, \mathbf{K}_0	3.1×10^3 /s	Rouchette et al. (2014)

The simulation parameters used here are listed in Table 1, if not specifically mentioned in the following simulations. The dimensionless equations can be obtained

after normalization in the same way adopted in the former section. Periodic boundary conditions were employed here, and continuous climbing of the GB dislocations was driven solely by the vacancy absorption due to the absence of external applied stress. The initial values of the phase field parameters η^R and η were obtained from the relaxation simulation in section 2.2. The initial vacancy concentration was chosen as its thermal equilibrium value, $c^{th} = \exp(-E^f / k_B T) = 1.2341 \times 10^{-4}$.

External applied stresses would have a significant effect on the absorption process at the GBs, although it is not studied here. The externally applied stresses have the climb component of the Peach-Koehler force on the GB dislocations $f_{cl} = -\sigma_{11} b$; thus, the equilibrium vacancy concentration at the dislocation core should be $c_d = c^{th} \exp(-f_{cl} V_m / b k_B T)$. The tension (compression) stress along the x-axis will increase (decrease) c_d , leading to a decrease (increase) of the sink strength.

3.2 Results and discussion

3.2.1 Sink behavior of tilt GBs in the PFM of dislocation climb

First, $K_0 = 0$ was adopted to test the sink performances of the GBs under the non-irradiation condition in the PFM of dislocation climb. In this situation, the system is unchanged from its initial state, indicating that the GB dislocations and vacancies are at their thermodynamic equilibrium state. Then, the sink processes are investigated under irradiation ($K_0 > 0$). Fig. 4 reveals the evolution of the calculated average concentration $\bar{c} = \int c dr^3 / V$ in the bi-crystal system with a $\theta = 2.86^\circ$ tilt boundary, and the computational size is $80b \times 80b \times 2b$. The vacancies are generated as a constant rate $K_0 = 3.1 \times 10^3 / s$ and absorbed by the GB dislocations. Initially the average vacancy concentration is at the thermal equilibrium value and then increases

rapidly due to the absorption rate being lower than the generation rate. However, the absorption rate also increases along with the increase in the average vacancy concentration, and then a steady state will be achieved when the absorption rate equals the generation rate. The insets in Fig. 4 exhibit the vacancy concentration fields at four different times. As shown in these insets, the vacancy concentration is at a minimum within the dislocation core and gradually changed around the core, revealing that the vacancies are absorbed at the dislocation cores. For a direct view of the dynamic motion of the climbing dislocations, Fig. 5 presents the calculated profiles of crystalline energy along the y axis at three different times corresponding to Fig. 4, and the peaks of the profiles show the locations of the dislocation cores. Fig. 5 clearly shows that the dislocations are moving in the negative direction of the y axis (see the green arrow line in the dashed red box). According to the climbing distance and the time step, the moving speed of the dislocations is $1.32 \times 10^{-3} \text{ m/s}$, which is comparable to that computed by Geslin et al. (2014). These findings reveal the physical process by which the GB absorbs vacancies through the dynamic climbing of the edge dislocation array.

Benefiting from the periodical condition in this model, the tilt GB would be infinitely long and the climbing of the parallel GB dislocations is continuous; thus, a dynamic steady state is obtained, and the sink strength is able to be calculated effectively. The continuous vacancy absorption process results in an infinite capacity of the GB in attracting vacancies. However, a tilt GB in polycrystalline materials cannot be infinitely long, and the climbing motion of all dislocations along one direction would reduce the GB dislocation density in certain areas. The vacancy absorption capacity of the GB will decline with the decrease in the GB dislocation density. Finally, the GB will disappear and no longer absorb vacancies.

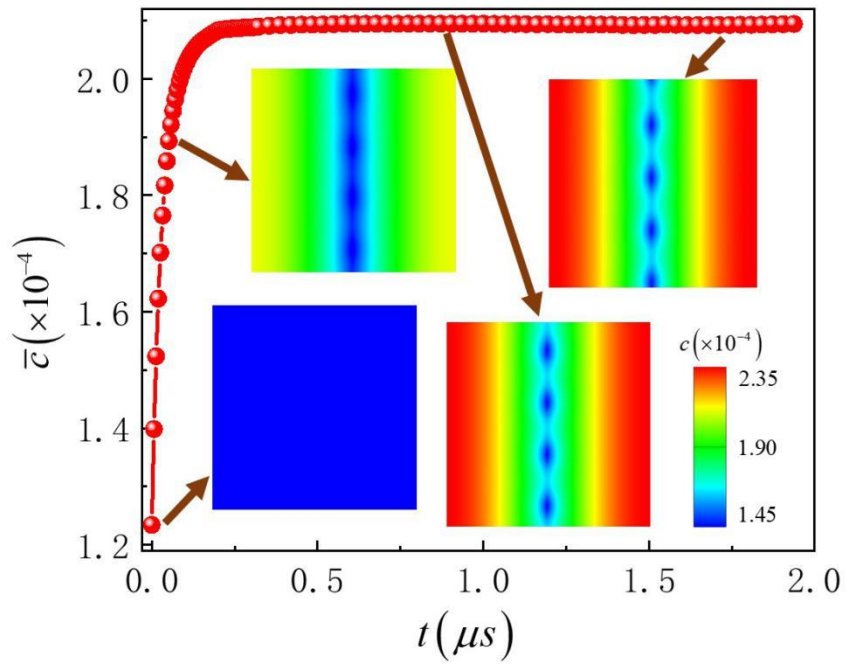


Fig. 4 Plots of the calculated average vacancy concentration with respect to time in the PFM of dislocation climb. The four insets show the vacancy concentration fields at different times. The circles in the insets represent the same dislocation at different times.

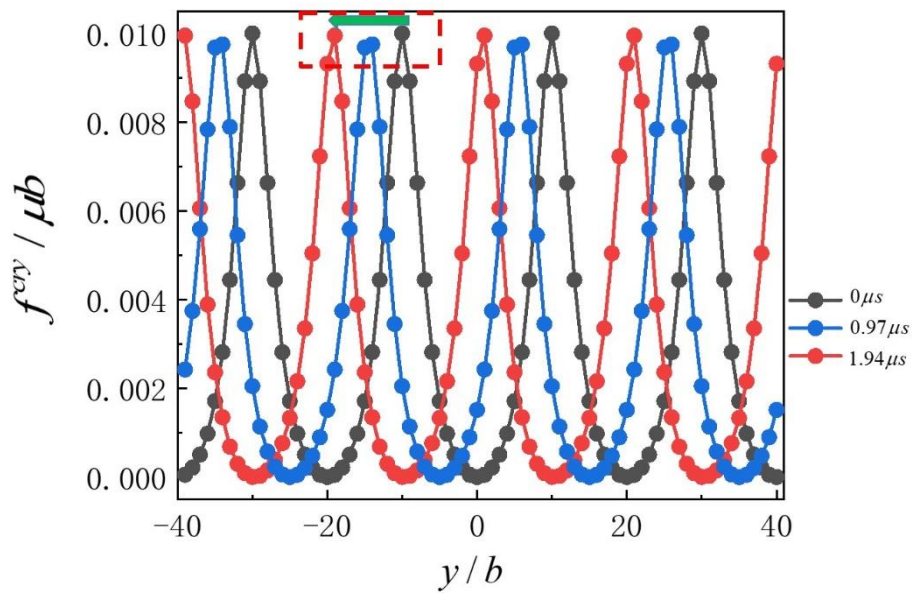


Fig. 5 The calculated profiles of crystalline energy $f^{cry} / \mu b$ with respect to y/b at three

different times corresponding to Fig. 4; the green arrow in the dashed red box shows the moving direction of the climbing dislocations.

The elastic interaction between dislocations and vacancies can be verified using the proposed dislocation climb model. The comparison between the vacancy concentration distribution and the hydrostatic stress field of the $\theta = 1^\circ$ GB is given by Fig. 6. The result clearly exhibits that the minimum vacancy concentration areas are located at the tensile stress regions near dislocation cores, as expected from the theoretical analysis.

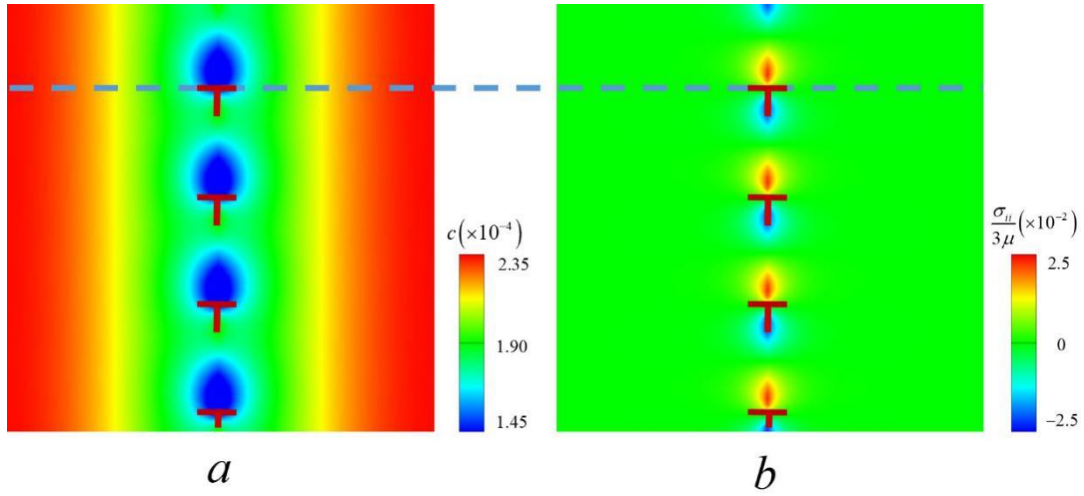


Fig. 6 a. Vacancy concentration distribution and **b.** Hydrostatic stress distribution at $t = 1.3\mu s$.

3.2.2 Sink strengths of tilt GBs

In the rate theory models (Was, 2007), the sink strength is the central parameter for quantifying the ability of the sink to absorb PDs. The sink strength k can be expressed by the average vacancy concentration \bar{c} at the steady state (Jiang et al., 2014; Rouchette et al., 2014):

$$k = \frac{K_0}{D(\bar{c} - c^h)}. \quad (18)$$

Since the steady state can be easily achieved in our PFM of the dislocation climb, we

may calculate the sink strengths of the GBs with different tilt angles. In this part of the simulations, the influence of the elastic vacancy-dislocation interaction was neglected by setting $\Delta V=0$ for simplicity. The computational cell was $80b \times 4h \times 2b$ with periodic boundary conditions. The cell size along the y axis was chosen as an integral multiple of the distance between the neighboring dislocations to ensure the accuracy of the calculated sink strength. The cell size along the x axis can be viewed as the grain size, which has a significant influence on the sink strength. Here, we fixed it at a constant value, and the detailed studies of the grain size effects (Gu et al., 2017; Jiang et al., 2014) have suggested that the GB's sink strength decreases with an increase in the grain size.

In the ideal sink model, compared to long-range vacancy diffusion, the short-range reactions between vacancies and dislocations are assumed to be very fast, such that the sink behavior is only controlled by the bulk diffusion of vacancies. However, the short-range reaction is related to the mechanism of vacancy absorption at dislocation jogs (Geslin et al., 2014). The vacancy-dislocation reaction rate should be limited if the jog formation energy is high; thus, the vacancy absorption process may be controlled by the short-range reaction rather than the bulk diffusion. The parameter of dislocation climbing mobility L^* represents the exchange rate of vacancy from the bulk to the dislocation core, i.e., the short-range reaction rate. Following the previous studies (Geslin et al., 2014; Ke et al., 2014), a dimensionless parameter L^* is defined as $L^* = Lb^2 / M_0$ to reflect the relative rate of the short-range reaction compared to the long-range vacancy bulk diffusion, where $M_0 = M(c^{th}) = V_m D c^{th} (1 - c^{th}) / (k_B T)$ is the mobility coefficient of the vacancy in the bulk. Thus, different values of L^* were applied to investigate the controlling mechanism of the vacancy absorption process.

The value of L can be obtained from atomistic simulations in principle and has been estimated by an asymptotic analysis of the vacancy diffusion profile at the level of dislocation jogs (Geslin et al., 2015):

$$L = \frac{2\pi dV_m Dc^{th} / (3wb^2 k_B T)}{\ln(r_c^{eff} / r_c) + (l_v^2 / r_c^2) \left\{ 1 + 2\alpha^2 \left[d_j / (2\alpha l_c) \coth \left[d_j / (2\alpha l_c) \right] - 1 \right] \right\}}, \quad (19)$$

where r_c^{eff} is the radius of the inner region of $c = c^{th}$, r_c is the dislocation core radius, while l_c and l_v are the typical diffusion lengths of a vacancy in the dislocation core and from the bulk to the dislocation core, respectively. α is a coefficient, and d_j is the separating distance between the regularly distributed dislocation jogs. With the assumption of high jog density, d_j is therefore small enough such that $d_j / (2\alpha l_c) \ll 1$ and $d_j / (2\alpha l_c) \coth \left[d_j / (2\alpha l_c) \right] \approx 1$. Substituting $r_c^{eff} \approx r_c = w$ and $M_0 = V_m Dc^{th} / (k_B T)$ into equation (19) gives:

$$L^* = \frac{Lb^2}{M_0} = \frac{2\pi dw}{3l_v^2}. \quad (20)$$

The characteristic length scale l_v is defined by $l_v^2 = (Dr_c / a\nu) \exp(E^{v-c} / k_B T)$, where a is the lattice parameter, ν is the Debye frequency, and E^{v-c} is the vacancy exchange energy barrier from the bulk to the dislocation core. Thus, L^* can be written as:

$$L^* = \frac{2\pi d a \nu}{3D_0} \exp \left[(E^m - E^{v-c}) / k_B T \right] \quad (21)$$

With $a = d$ and $\nu = 9.3 \times 10^{13}$ /s (Geslin et al., 2015), L^* is estimated by:

$$L^* \approx \exp \left[(E^m - E^{v-c}) / k_B T \right] \quad (22)$$

This clearly shows that L^* is associated with the difference between the energy barriers for the vacancy bulk diffusion E^m and the ‘‘short-range reaction’’ E^{v-c} . From the atomistic calculations in Kabir et al. (2010) and the related discussions in Niu et al.

(2017), the values are $E^m - E^{v-c} = 0.35$ eV and -0.04 eV along two typical vacancy migration paths for the $\langle 111 \rangle$ (110) 71° edge-type dislocations in bcc iron, resulting in $L^* = 148.4$ and 0.56 at $T = 812$ K for the two corresponding cases, respectively. Although such results are obtained for metal iron, it is believed that these atomistic results also indicate a similar wide range of possible values of L^* for other materials.

Because of the wide range of L^* , Ke et al. (2014) chose $L^* = 1, 2, 4, 10$ and 100 to study the climb velocity of a single edge dislocation. We also adopted the same values of L^* and applied them to the coupled reaction-diffusion dislocation climb model to investigate the sink strengths of GBs with tilt angles less than 10° , and the results are compared to that of the ideal sink model. The calculated sink strengths with respect to the tilt angles by the two models are shown in Fig. 7. The sink strength of a perfect planar sink is also presented in this figure, and its analytical solution is given by $k^{\text{perfect}} = 12 / (R - 2r_0)^2$ in the literature (Jiang et al., 2014), where R is the grain size and r_0 is the width of the sink. In this study, $R = 80b$ and $r_0 = 0$ (the perfect planar sink is strictly confined within the GB with zero thickness); thus, $k^{\text{perfect}} = 0.0231 \text{ nm}^{-2}$.

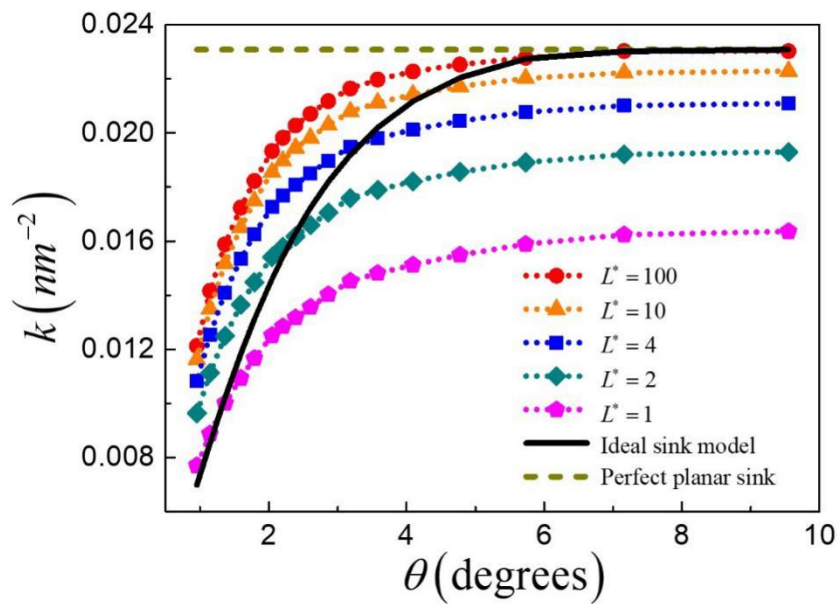


Fig. 7 Plots of the calculated sink strengths with respect to the tilt angles by the dislocation climb model and the ideal sink model. The dashed line represents the sink strength of the perfect planar sink.

All of the curves obtained by the two models demonstrate that sink strength increases with the increase in the tilt angle, as shown in Fig. 7, agreeing with the previous studies (Jiang et al., 2014). As observed in the results calculated by the dislocation climb model, it is easy to find that sink strength decreases with the decrease in L^* for an arbitrary angle. For the cases with small L^* , the short-range vacancy-dislocation reaction rate is limited, and the sink behavior is reaction-controlled, which results in lower sink strengths. As the values of L^* increase, the sink strengths calculated by the dislocation climb model increase and gradually converge, indicating that the influences of L^* on the sink processes are weakened. Larger L^* values reflect faster short-range reactions, and the sink strength is mainly determined by the long-range vacancy diffusion. By using the different kinetic coefficients to represent the mean absorbing rate of the dislocations to vacancies, the transformation from reaction-controlled to the diffusion-controlled sink behaviors is accessible.

In Fig. 7, the results of the dislocation climb model with $L^*=100$ show a good agreement with that of the ideal sink model at relatively high tilt angles because both cases are controlled by vacancy diffusion. The numerically calculated sink strengths of these GBs are consistent with the analytical solution of the perfect planar sink, indicating the validation of the two models at high tilt angles employed in this study. However, for relatively low tilt angles, significant differences exist between the two models even when diffusion control is the dominant mechanism. To better understand the reasons, detailed vacancy concentration fields at the steady states calculated by the two models for $\theta=2.86^\circ$ and 7.16° are displayed in Fig. 8. For the case of $\theta=2.86^\circ$, the dynamic motion of the dislocation sinks in the dislocation climb model results in continuous regions of low vacancy concentration along the GB, while areas of low concentration in the ideal sink model are located at isolated dislocation cores. Thus, the

average vacancy concentration in GB in the dislocation climb model is lower, and the calculated sink strength is higher. When the tilt angle is 7.16° , the dislocation density is high in the GB and the effect of dynamic motion of dislocations is not significant. Thus, sink strengths calculated by the two models are similar when diffusion control is dominant. This result reveals that the dynamic motion of dislocations is an important factor that influences the sink strength of GBs, especially for the ones with low misorientation angles and high PD absorption rates.

This clearly shows that the calculated sink strength changes by approximately a factor of 2 for all the considered cases from Fig. 7. The effect of such a change on the widely used rate theory models will be evaluated in the following. The time-dependent ‘‘mean field’’ rate-theory equation for the evolution of the average vacancy concentration is:

$$\frac{d\bar{c}}{dt} = K_0 - kD(\bar{c} - c^{th}). \quad (23)$$

Since $\bar{c} = c^{th}$ at $t = 0$, the solution to this equation is:

$$\bar{c} = \frac{K_0}{kD} [1 - \exp(-kDt)] + c^{th} \quad (24)$$

According to equation (24), Fig. 9 plots the average vacancy concentration as a function of time at $k = 0.01 \text{ nm}^{-2}$ and 0.02 nm^{-2} with $K_0 = 10^7 \text{ /s}$ (high dose irradiation environments). The large difference between the two curves in Fig. 9 shows that the rate theory models are very sensitive to the change in sink strength in Fig. 7. Void nucleation is allowed when the vacancy concentration equals a critical value c^{cr} , and Millett et al. (2009) have estimated the critical value to be within $0.3 < c^{cr} < 0.35$. If $c^{cr} = 0.3$ is chosen here, as shown in Fig. 9, the phenomenon of void nucleation can happen at $t = 0.056 \text{ } \mu\text{s}$ for $k = 0.01 \text{ nm}^{-2}$ but will never emerge for $k = 0.02 \text{ nm}^{-2}$. These results indicate that it is necessary to consider the dislocation climb process for

evaluating the radiation-resistant ability of a GB.

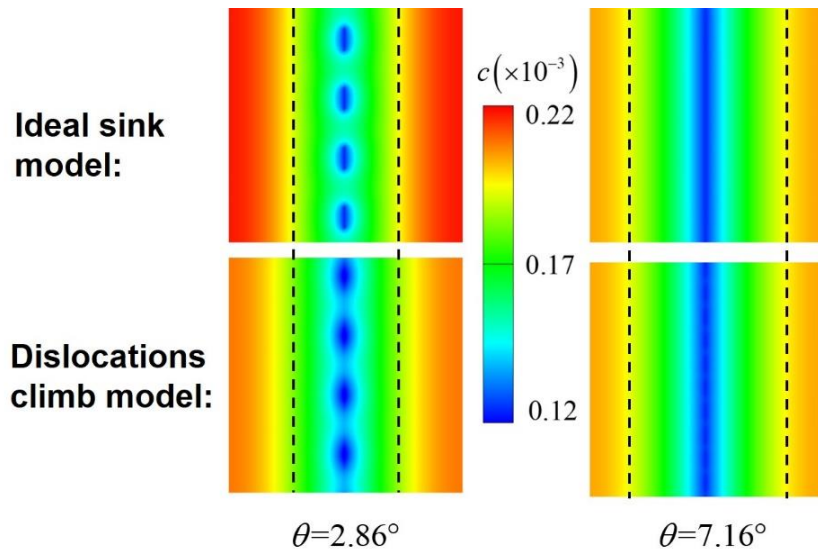


Fig. 8 Detailed vacancy concentration fields at the steady states calculated by the two models for $\theta = 2.86^\circ$ and $\theta = 7.16^\circ$. The results of the dislocation climb model are obtained with $L^* = 100$.

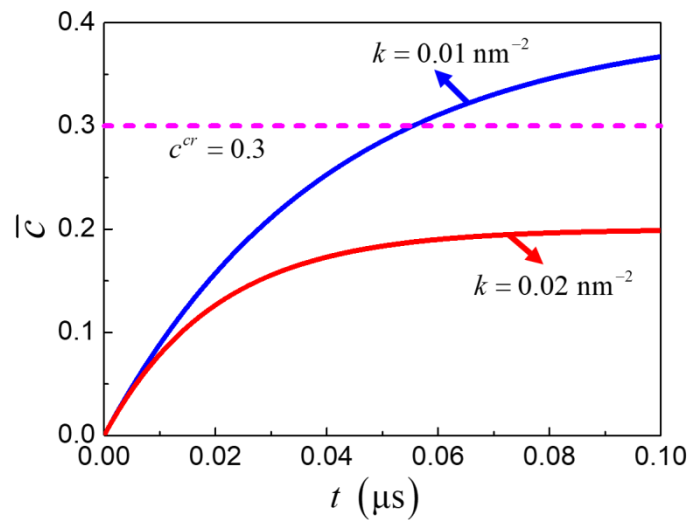


Fig. 9 Plots the average vacancy concentration \bar{c} as a function of time at $k = 0.01 \text{ nm}^{-2}$ and 0.02 nm^{-2} with $K_0 = 10^7 / \text{s}$.

4. Summary

The PFM of the dislocation climb for describing the structures of low-angle symmetrical tilt GBs was developed in this work and then applied to evaluate GB sink behaviors for PDs. A steady state was achieved so that the vacancy generation due to the irradiation can be balanced by vacancy absorption via the dynamic motion of the climbing GB dislocations. The average vacancy concentration at the steady state was used to calculate the sink strength corresponding to the rate theory. The ideal sink model that assumes a fixed vacancy concentration within the immobile dislocation cores is also presented here for comparison. The results simulated by the dislocation climb model show that the GB sink strengths are not only determined by the long-range vacancy diffusions but also the short-range reactions between vacancies and dislocations. A transition from reaction-controlled to diffusion-controlled sink behaviors is accessible in the dislocation climb model, in contrast to the merely diffusion-controlled sink processes in the ideal sink model. In addition, dynamic motion of the GB dislocations in the dislocation climb model exhibits significant effects on the GB sink strength, indicating that the creep deformation of the GB's microstructure must be considered to predict the ability of GBs to absorb radiation defects.

Acknowledgments

This work was supported by the National Key R&D Program of China (No. 2017YFB0702404), the National Natural Science Foundation of China (No. 51672232), and the Research Grants Council of Hong Kong (PolyU 152636/16E). The authors thank Prof. Yao Shen from Shanghai Jiao Tong University for valuable expert discussions.

References

- Ayas, C., Van Dommelen, J. A. W., Deshpande, V. S., 2014. Climb-enabled discrete dislocation plasticity. *J. Mech. Phys. Solids* 62, 113-136.
- Babu, B., Lindgren, L. E., 2013. Dislocation density based model for plastic deformation and globularization of Ti-6Al-4V. *Int. J. Plasticity* 50, 94-108.
- Bai, X. M., Voter, A. F., Hoagland, R. G., Nastasi, M., Uberuaga, B. P., 2010. Efficient annealing of radiation damage near grain boundaries via interstitial emission. *Science* 327, 1631-1634.
- Bai, X. M., Vernon, L.J., Hoagland, R.G., Voter, A.F., Nastasi, M., Uberuaga, B.P., 2012. Role of atomic structure on grain boundary-defect interactions in Cu. *Phys. Rev. B* 85, 214103.
- Basirat, M., Shrestha, T., Potirniche, G. P., Charit, I., Rink, K., 2012. A study of the creep behavior of modified 9Cr-1Mo steel using continuum-damage modeling. *Int. J. Plasticity* 37, 95-107.
- Beyerlein, I.J., Demkowicz, M.J., Misra, A., Uberuaga, B.P., 2015. Defect-interface interactions. *Prog. Mater. Sci.* 74, 125-210.
- Beyerlein, I. J., Hunter, A., 2016. Understanding dislocation mechanics at the mesoscale using phase field dislocation dynamics. *Phil. Trans. R. Soc. A* 374, 20150166.
- Bobylev, S. V., Mukherjee, A. K., Ovid'ko, I. A., Sheinerman, A. G., 2010. Effects of intergrain sliding on crack growth in nanocrystalline materials. *Int. J. Plasticity* 26, 1629-1644.
- Bringa, E.M., Monk, J.D., Caro, A., Misra, A., Zepeda-Ruiz, L., Duchaineau, M., Abraham, F., Nastasi, M., Picraux, S.T., Wang, Y.Q., 2011. Are nanoporous materials radiation resistant? *Nano Lett.* 12, 3351-3355.
- Dai, S., Xiang, Y., Srolovitz, D.J., 2013. Structure and energy of (111) low-angle twist boundaries in Al, Cu and Ni. *Acta Mater.* 61, 1327-1337.
- Davoudi, K. M., Nicola, L., Vlassak, J. J., 2012. Dislocation climb in two-dimensional discrete dislocation dynamics. *J. Appl. Phys.* 111, 103522.
- Demkowicz, M. J., Misra, A., Caro, A., 2012. The role of interface structure in controlling high helium concentrations. *Curr. Opin. Solid State Mater. Sci.* 16, 101-108.
- Fischer, F. D., Svoboda, J., 2011. Chemically and mechanically driven creep due to generation and annihilation of vacancies with non-ideal sources and sinks. *Int. J. Plasticity* 27, 1384-1390.
- Gao, Y., Zhuang, Z., Liu, Z. L., You, X. C., Zhao, X. C., Zhang, Z. H., 2011. Investigations of pipe-diffusion-based dislocation climb by discrete dislocation dynamics. *Int. J. Plasticity* 27, 1055-1071.
- Geers, M.G.D., Cottura, M., Appolaire, B., Busso, E.P., Forest, S., Villani, A., 2014. Coupled glide-climb diffusion-enhanced crystal plasticity. *J. Mech. Phys. Solids* 70, 136-153.

- Geslin, P. A., Appolaire, B., Finel, A., 2014. A phase field model for dislocation climb. *Appl. Phys. Lett.* 104, 011903.
- Geslin, P. A., Appolaire, B., Finel, A., 2015. Multiscale theory of dislocation climb. *Phys. Rev. Lett.* 115, 265501.
- Gu, Y., Han, J., Dai, S., Zhu, Y., Xiang, Y., Srolovitz, D.J., 2017. Point defect sink efficiency of low-angle tilt grain boundaries. *J. Mech. Phys. Solids* 101, 166-179.
- Han, W.Z., Demkowicz, M.J., Fu, E.G., Wang, Y.Q., Misra, A., 2012. Effect of grain boundary character on sink efficiency. *Acta Mater.* 60, 6341-6351.
- Huang, M., Li, Z., Tong, J., 2014. The influence of dislocation climb on the mechanical behavior of polycrystals and grain size effect at elevated temperature. *Int. J. Plasticity* 61, 112-127.
- Jiang, C., Swaminathan, N., Deng, J., Morgan, D., Szlufarska, I., 2014. Effect of grain boundary stresses on sink strength. *Mater. Res. Lett.* 2, 100-106.
- Kabir, M., Lau, T. T., Rodney, D., Yip, S., Van Vliet, K. J., 2015. Predicting dislocation climb and creep from explicit atomistic details. *Phys. Rev. Lett.* 105, 095501.
- Ke, J.H., Boyne, A., Wang, Y., Kao, C.R., 2014. Phase field microelasticity model of dislocation climb: Methodology and applications. *Acta Mater.* 79, 396-410.
- Kenik, E. A., Busby, J. T., 2012. Radiation-induced degradation of stainless steel light water reactor internals. *Mater. Sci. Eng. R Rep.* 73, 67-83.
- Keralavarma, S. M., Cagin, T., Arsenlis, A., Benzerga, A. A., 2012. Power-law creep from discrete dislocation dynamics. *Phys. Rev. Lett.* 109, 265504.
- Lebensohn, R. A., Hartley, C. S., Tomé, C. N., Castelnau, O., 2010. Modeling the mechanical response of polycrystals deforming by climb and glide. *Phil. Mag.* 90, 567-583.
- Levitas, V.I., Lee, D.-W., Preston, D.L., 2010. Interface propagation and microstructure evolution in phase field models of stress-induced martensitic phase transformations. *Int. J. Plasticity* 26, 395-422.
- Li, Y., Hu, S., Sun, X., Stan, M., 2017. A review: applications of the phase field method in predicting microstructure and property evolution of irradiated nuclear materials. *npj Comput. Mater.* 3.
- Millett, P.C., Aidhy, D.S., Desai, T., Phillpot, S.R., Wolf, D., 2009. Grain-boundary source/sink behavior for point defects: an atomistic simulation study. *Int. J. Mater. Res.* 100, 550-555.
- Millett, P.C., Rokkam, S., El-Azab, A., Tonks, M., Wolf, D., 2009. Void nucleation and growth in irradiated polycrystalline metals: a phase-field model. *Modelling Simul. Mater. Sci. Eng.* 17, 064003.
- Misra, A., Demkowicz, M.J., Zhang, X., Hoagland, R.G., 2007. The radiation damage tolerance of ultra-high strength nanolayered composites. *JOM* 59, 62-65.

- Mordehai, D., Clouet, E., Fivel, M., Verdier, M., 2008. Introducing dislocation climb by bulk diffusion in discrete dislocation dynamics. *Phil. Mag.* 88, 899-925.
- Niu, X., Luo, T., Lu, J., Xiang, Y., 2017. Dislocation climb models from atomistic scheme to dislocation dynamics. *J. Mech. Phys. Solids* 99, 242-258.
- Odette, G. R., Alinger, M. J., Wirth, B. D., 2008. Recent developments in irradiation-resistant steels. *Annu. Rev. Mater. Res.* 38, 471-503.
- Rouchette, H., Thuinet, L., Legris, A., Ambard, A., Domain, C., 2014. Quantitative phase field model for dislocation sink strength calculations. *Comput. Mater. Sci.* 88, 50-60.
- Shen, C., Li, J., Wang, Y., 2014. Predicting structure and energy of dislocations and grain boundaries. *Acta Mater.* 74, 125-131.
- Tschopp, M.A., Solanki, K.N., Gao, F., Sun, X., Khaleel, M.A., Horstemeyer, M.F., 2012. Probing grain boundary sink strength at the nanoscale: Energetics and length scales of vacancy and interstitial absorption by grain boundaries in α -Fe. *Phys. Rev. B* 85, 064108.
- Wan, H., Shen, Y., Jin, X., Chen, Y., Sun, J., 2012. Effects of coherency stress and vacancy sources/sinks on interdiffusion across coherent multilayer interfaces—Part I: Theory. *Acta Mater.* 60, 2528-2538.
- Wang, J., Beyerlein, I. J., Tomé, C. N., 2014. Reactions of lattice dislocations with grain boundaries in Mg: implications on the micro scale from atomic-scale calculations. *Int. J. Plasticity* 56, 156-172.
- Wang, Y., Li, J., 2010. Phase field modeling of defects and deformation. *Acta Mater.* 58, 1212-1235.
- Was, G.S., 2007. *Fundamentals of radiation materials science: metals and alloys*. Springer, Berlin.
- Yu, W., Shen, S., 2016. Energetics of point defect interacting with grain boundaries undergone plastic deformations. *Int. J. Plast.* 85, 93-109.
- Zeng, Y., Hunter, A., Beyerlein, I. J., Koslowski, M., 2016. A phase field dislocation dynamics model for a bicrystal interface system: An investigation into dislocation slip transmission across cube-on-cube interfaces. *Int. J. Plasticity* 79, 293-313.
- Zhang, Y., Huang, H., Millett, P.C., Tonks, M., Wolf, D., Phillpot, S.R., 2012. Atomistic study of grain boundary sink strength under prolonged electron irradiation. *J. Nucl. Mater.* 422, 69-76.
- Zheng, S., Ni, Y., He, L., 2015. Phase field modeling of a glide dislocation transmission across a coherent sliding interface. *Modell. Simul. Mater. Sci. Eng.* 23, 035002.
- Zheng, S., Zheng, D., Ni, Y., He, L., 2018. Improved phase field model of dislocation intersections. *npj Comput. Mater.* 4, 20.